NANO LETTERS

Letter

pubs.acs.org/NanoLett

Probing Redox Reactions at the Nanoscale with Electrochemical Tip-Enhanced Raman Spectroscopy

Dmitry Kurouski,[†] Michael Mattei,[†] and Richard P. Van Duyne*[,†,‡]

[†]Department of Chemistry and [‡]Applied Physics Program, Northwestern University, Evanston, Illinois 60208, United States

Supporting Information

ABSTRACT: A fundamental understanding of electrochemical processes at the nanoscale is crucial to solving problems in research areas as diverse as electrocatalysis, energy storage, biological electron transfer, and plasmon-driven chemistry. However, there is currently no technique capable of directly providing chemical information about molecules undergoing heterogeneous charge transfer at the nanoscale. Tip-enhanced Raman spectroscopy (TERS) uniquely offers subnanometer spatial resolution and single-molecule sensitivity, making it the ideal tool for studying nanoscale electrochemical processes with high chemical specificity. In this work, we demonstrate the first electrochemical TERS (EC-TERS) study of the nanoscale redox behavior of Nile Blue (NB), and compare these results with conventional cyclic voltammetry (CV). We successfully monitor the disappearance of the 591 cm^{-1} band of NB upon reduction and its reversible reappearance upon oxidation during the CV. Interestingly, we observe a negative shift of more than 100 mV in the onset of the potential response of the TERS intensity of the 591 cm^{-1} band, compared to the onset of faradaic current in the CV. We hypothesize that perturbation of the electrical double-layer by the TERS tip locally alters the effective potential experienced by NB molecules in the tip−sample junction. However, we demonstrate that the tip has no effect on the local charge transfer kinetics. Additionally, we observe step-like behavior in some TERS voltammograms corresponding to reduction and oxidation of single or few NB molecules. We also show that the coverage of NB is nonuniform across the ITO surface. We conclude with a discussion of methods to overcome the perturbation of the double-layer and general considerations for using TERS to study nanoscale electrochemical processes.

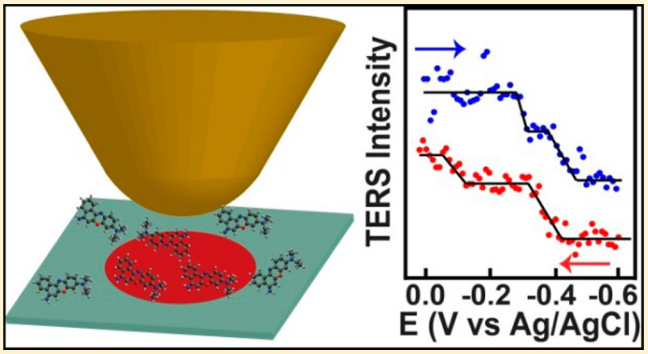

KEYWORDS: *Tip-Enhanced Raman Spectroscopy (TERS), Nanoscale Electrochemistry, Cyclic Voltammetry (CV)*

Unraveling electrochemical process at the nanoscale is critical for understanding how electrode surface heterogeneity locally affects electron transfer processes in range of fields,[1] including electrocatalysis[2−5] and biological electron transfer.[6] Electrochemical scanning probe techniques such as scanning electrochemical microscopy (SECM)[7,8] and electrochemical scanning tunneling microscopy (EC-STM)[9,10] provide nanoscale information about electrode surface structure. For example, Sun et al. recently demonstrated SECM imaging of the catalytic activity of individual Au nanoparticles with ∼10 nm spatial resolution.[8] EC-STM can achieve submolecular resolution imaging of the potential dependent configurations of adsorbed electroactive molecules, such as porphyrins, on a well-defined electrode surface.[10] However, neither technique provides direct chemical information about the molecules undergoing nanoscale electron transfer reactions. Spectroscopic techniques, such as surface-enhanced Raman spectroscopy (SERS) and fluorescence microscopy, offer such chemical information and have been used to optically probe nanoscale electrochemical processes involving single molecules.[11−14] For example, Cortés et al. recently demonstrated that oxidation and reduction of a single molecule can be observed using SERS and that the potentials at which single molecule redox events occur depend strongly on the local surface environment.[11] However, neither SERS nor fluorescence microscopy is capable of selectively monitoring electrochemical processes at a particular location of interest in the electrode surface. Clearly, a technique is needed which can combine the high spatial resolution electrochemical mapping provided by SECM and EC-STM with the sensitivity and selectivity of SERS to elucidate the effects of nanoscale electrode features on local heterogeneous charge transfer.

Tip-enhanced Raman spectroscopy (TERS) is a powerful tool that exploits the localized surface plasmon resonance (LSPR) of a Ag or Au scanning probe to locally enhance the Raman scattering of molecules in the tip−sample junction by at least a factor of 10^6.[15−19] Its unique combination of subnanometer spatial resolution, single-molecule sensitivity, and rich vibrational information makes TERS the ideal tool for studying redox reactions at the nanoscale.[20−23] Recently, the

Received: July 31, 2015
Revised: November 4, 2015
Published: November 18, 2015

DOI: 10.1021/acs.nanolett.5b04177
Nano Lett. 2015, 15, 7956−7962

utility of TERS for monitoring and spectroscopically mapping reactions at the nanoscale was demonstrated using the photocatalytic conversion of *p*-nitrothiophenol to *p*,*p*′-dimercaptoazobisbenzene.[24−26] Extending TERS to electrochemical environments would uniquely provide chemically specific imaging of redox processes across nanoscale electrode features. TERS has been demonstrated previously in an aqueous environment[27] and very recently under electrochemical conditions,[28] but probing an electrochemical reaction with TERS has not yet been realized. In this work, we demonstrate, for the first time, the use of TERS for directly monitoring of the structural changes of a redox active molecule during the electron transfer process in the nanoscale tip−sample junction. We then discuss the major challenges to using electrochemical TERS (EC-TERS) for nanoscale mapping of heterogeneous charge transfer processes.

ITO coverslips (18 × 18 mm, 8−12 Ω, SPI Supplies) were cleaned by sonication in pure ethanol (VWR International) for 30 min. After the coverslips were dried under argon flow, a few drops of 170 μM ethanolic solution of NB (Sigma-Aldrich) was placed on their surface and exposed for 3−4 s. The excess of NB solution was removed from the ITO by thorough rinsing with pure ethanol. The coverslips were then dried under argon flow. The ITO coverslip (working electrode) was fixed at the bottom of the 2 mm Kel-F wet-cell (Agilent, Supporting Information (SI) Figure S1) and sealed by epoxy (Araldite 2043). A silver wire (0.25 mm diameter, Alfa Aesar) was attached to the top of ITO film by silver epoxy (Ted Pella) to achieve external electrical contact. Both the silver epoxy and the Ag wire were insulated from the working solution using Araldite. Pt (0.5 mm diameter, Alfa Aesar) and Ag/AgCl wires were used as the counter electrode and reference electrode, respectively. The working solution was 50 mM Tris buffer containing 50 mM NaCl (pH 7.1, both compounds purchased from Sigma-Aldrich). The Ag/AgCl wire reference electrode was directly immersed in the supporting electrolyte containing 50 mM Cl^-. Therefore, all potentials are referenced to Ag/AgCl (50 mM NaCl).

TERS probes were prepared by thermal evaporation (PVD 75, Kurt J. Lesker, Efferson Hills, PA) of a 70 nm Au film at a rate of 0.5 Å/s onto contact mode AFM cantilevers (NanoandMore USA). All EC-TER spectra were acquired on a home-built microscope system (SI Figure S1).[18] A 633 nm continuous wave laser (Spectra Physics) was used as the excitation source. Laser power was adjusted with a neutral density filter wheel (ThorLabs) and was directed into the back port of an inverted Nikon TE-2000U microscope, reflected off of a 10/90 beam splitter, and directed upward into 1.3 NA 100× oil-immersed Nikon objective. Laser powers at the sample ranged from 70 to 110 μW. An Agilent Molecular Imaging PicoPlus AFM was mounted on a Prior Scientific stage for AFM imaging and *X*−*Y* laser positioning, respectively. After the TER tip was approached to the ITO surface, the laser was focused on the tip apex using a Renishaw stage (*X* and *Y* directions) and microscope objective (*Z* direction). The AFM scanner implemented an IR diode feedback laser, which prevents spectral interference in TERS measurements. The scattered light was collected through the Nikon objective, passed through a long-pass filter (LP03-633RS-25, Semrock) to filter Rayleigh light and was directed to a confocal Raman spectrometer (Princeton Instruments, SP2500i) equipped with a 600 groove/mm grating and a slit entrance set to 100 μm. The dispersed light was then sent to a liquid nitrogen-cooled PI-Acton Spec-10 CCD for spectral acquisition. The potential of the ITO surface was controlled by a bipotentiostat (CH Instruments). To demonstrate that the TER tip is not contaminated with NB molecules, the ITO working electrode was retracted at the end of each experiment such that the apex of the TER tip would still be in the focus of the excitation laser (SI Figure S2). The absence of Raman lines corresponding to NB in the spectrum taken after retraction demonstrates that the TER tip was not contaminated. When tip contamination does occur, Raman lines corresponding to NB are observed in the retracted spectrum (SI Figure S2, left panel). In such a case, the EC-TERS results so acquired were disregarded.

Gold-film-over-nanosphere (Au FON) electrodes were prepared by drop casting 4 μL of 0.05% Triton X (aq) and 0.5 μL of 280 nm polystyrene spheres (Bangs Laboratories, Inc.) onto 2 mm diameter commercial Au disk electrodes (CH Instruments) by a similar procedure as previously described.[29] A 150 nm Au film was deposited on top of the spheres at a rate of 0.5 Å/s using a thermal deposition system (Kurt J. Lesker). The Au FON was mounted into a stainless steel electrochemical cell fit with a Pt counter electrode and Ag/AgCl wire reference electrode. Tris buffer (50 mM Tris, 50 mM NaCl, pH = 7.1) was degassed with argon before injection into the cell. Surface-enhanced Raman (SER) spectra were acquired on an inverted microscope (Nikon Eclipse Ti−U) with a 50× objective (NA = 0.55) A 633 nm He−Ne laser (Research Electro-Optics) was directed into the back port of the microscope and reflected by a beamsplitter into the objective. The scattered light was collected through the same objective, and filtered (LP03-633RS-25, Semrock). The light was then focused into a 1/3 m spectrograph (SP2300, Princeton Instruments), dispersed (1200 grooves/nm, 500 nm blaze), and imaged with a liquid N_2-cooled CCD camera (Spec10:400BR, Princeton Instruments).

A double-beam spectrophotometer (Cary 5000, Agilent) was used to measure absorbance spectra of 10 μM oxidized and reduced NB in phosphate buffer (pH = 7.1, Sigma-Aldrich). Nile blue was chemically reduced using 0.1 M sodium ditihionite (Sigma-Aldrich). MATLAB and GRAMS/AI 7.0 were used for all data processing. All potentials are quoted relative to Ag/AgCl.

To demonstrate the feasibility of electrochemical TERS, the redox dye Nile blue (NB) was chosen as a prototypical molecule. NB undergoes a two-electron one-proton reduction at pH > 6, as demonstrated previously by Ni et al. (Scheme 1).[30]

Scheme 1. Redox Reaction of NB at pH > 6

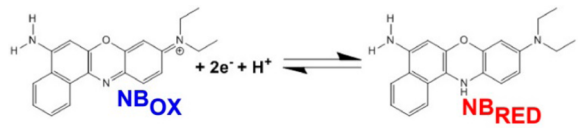

As shown in Figure 1, the reduced and oxidized forms of NB (NB_{RED} and NB_{OX}) have distinctive features in their respective UV−vis absorption spectra. Most notably, the disruption of the conjugation in the central ring of NB upon its reduction results in the disappearance of the strong absorption features at 602 and 634 nm (Figure 1). NB_{RED} absorbs most strongly in the blue and near-UV regions, with prominent features at 261, 362, and 405 nm. In our EC-TERS experiment, we used 633 nm

DOI: 10.1021/acs.nanolett.5b04177
Nano Lett. 2015, 15, 7956−7962

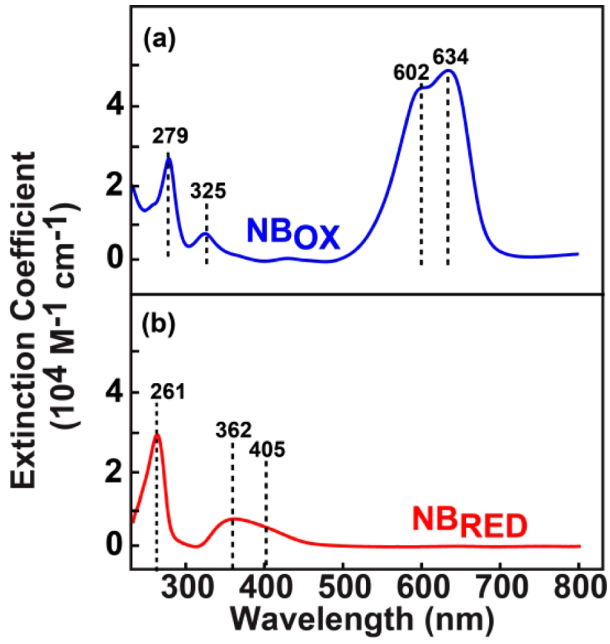

Figure 1. UV−vis spectra of oxidized (NB_{OX}, (a)) and reduced (NB_{RED}, (b)) NB. NB_{RED} was produced by chemical reduction of NB_{OX} with sodium dithionite. The extinction coefficients of NB_{OX} (M^{-1} cm^{-1}) at the following wavelengths are λ = 279 nm, ϵ = 26 000; λ = 325 nm, ϵ = 7300; λ = 602 nm, ϵ = 43 000; λ = 634 nm, ϵ = 47 000. For NB_{RED}, the extinction coefficients (M^{-1} cm^{-1}) at various wavelengths are λ = 261 nm, ϵ = 24 000; λ = 362 nm, ϵ = 5800; λ = 405 nm, ϵ = 3800; λ = 633 nm, ϵ = 100.

continuous wave excitation to exploit the resonance Raman effect for probing NB_{OX}. Therefore, the Raman spectra of NB_{OX} reported in this work are tip-enhanced resonance Raman (TERR) and surface-enhanced resonance Raman (SERR) spectra. For simplicity, we will refer to spectra of both NB_{OX} and NB_{RED} as TER and SER spectra throughout this manuscript.

Using the apparatus shown in SI Figure S1, we acquired TER spectra of NB_{OX} at various applied potentials. Representative TER and EC-SER spectra of NB_X and NB_{RED} acquired at applied potentials of 0.0 V and −0.6 V, respectively, are shown along with corresponding SER spectra in Figure 2a. The EC-TER and EC-SER spectra are in good agreement with each other. The majority of NB_{OX} bands experience very small (1−3 cm^{-1}) shifts upon reduction. These shifts are consistent with the changes assigned to NB_{RED} by Ni et al. using SERS with 488 nm excitation[30] and by Cortés et al. using SERS with 633 nm excitation.[31] Notably, Cortés et al. also observed that the 591 and 1641 cm^{-1} bands of NB_{OX} are only about 1 order of magnitude more intense than those of NB_{RED} at 633 nm, despite the strong electronic resonance of NB_{OX} at this wavelength. We observe a comparable decrease in Raman intensity for these two bands upon NB reduction. Following literature precedent, we therefore tentatively assign the spectra acquired at −0.6 V vs Ag/AgCl to NB_{RED}. Quantitative vibrational assignments of NB_{OX} and NB_{RED} using time-dependent density functional theory (TD-DFT) are currently underway in our lab to verify our detection of NB_{RED}. In lieu of these theoretical assignments, qualitative vibrational assignments from the literature are given for NB_{OX} in SI Table S1.

There are several more prominent changes in the spectrum, which are highlighted in Figure 2b and c. The difference spectra (black curves) in these two panels highlight the most pronounced spectral changes. In Figure 2c, the 1376 cm^{-1} mode is much more intense relative to the 1354 cm^{-1} band for NB_{RED} than for NB_{OX}. Further, the 1354 cm^{-1} band of NB_{OX} shifts by 5 cm^{-1} to 1349 cm^{-1} in the spectrum of NB_{RED}. The shoulder at 1193 cm^{-1} in the spectrum of NB_{OX} also shifts by 10 cm^{-1} to 1203 cm^{-1} for NB_{RED}. A full list of spectral changes resulting from reduction is given in SI Table S1. Additionally, it is important to note that there are differences in the TER spectra of NB_{OX} and NB_{RED} relative to the corresponding SER spectra. For example, the relative intensities of the 1376 and 1585 cm^{-1} bands in the SER spectra of NB_{RED} are much larger than in the TER spectra. We attribute these discrepancies to differences in the binding strength and orientation of NB on the ITO vs Au surface. However, both the TERS spectra and the SERS spectra show consistent changes in the spectra of NB_{RED} relative to NB_{OX}. Therefore, differences in molecule−surface interactions on ITO and Au do not appear to significantly affect the potential response. All differences

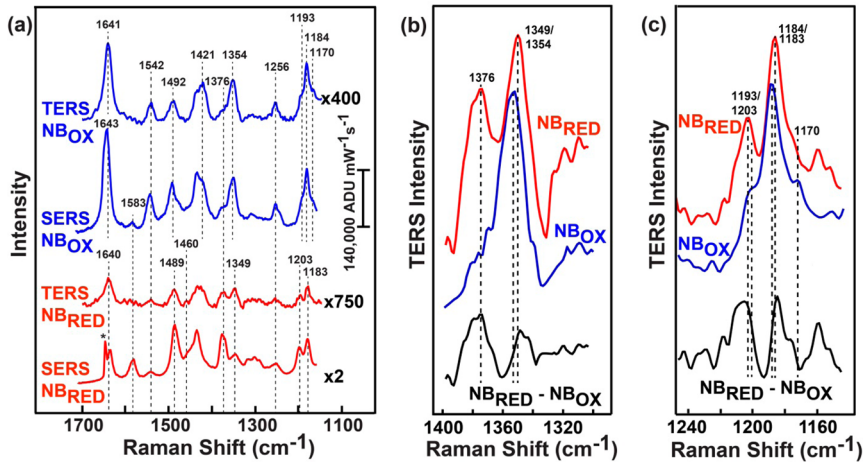

Figure 2. (a) EC-TER (on ITO) and EC-SER (on Au) spectra of NB_{OX} (blue) and NB_{RED} (red) vs Ag/AgCl. The asterisk denotes leaked room light. (b) and (c) Selected regions of the EC-TER spectra of NB_{OX} (blue) and NB_{RED} (red) vs Ag/AgCl and difference spectra (black) highlighting spectral changes in NB resulting from reduction. Spectra in (b) and (c) are normalized such that the 1354 and 1184 cm^{-1} bands have the same intensity for both species. All spectra are offset along the intensity axis for clarity.

DOI: 10.1021/acs.nanolett.5b04177
Nano Lett. 2015, 15, 7956−7962

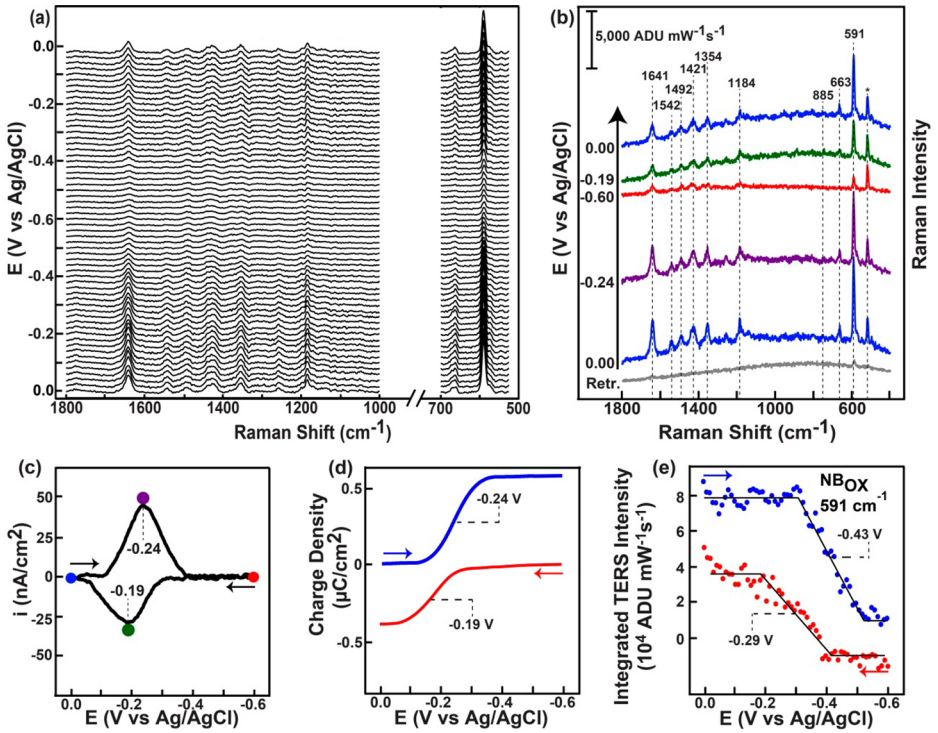

Figure 3. Stack plot (a) and individual (b) EC-TER spectra of NB acquired at different potentials during cyclic voltammetry (CV) showing reversible reduction and oxidation of NB. P = 110 μW, t = 1 s, λ = 633 nm, scan rate = 10 mV/s. The asterisk denotes the Si Raman band from the AFM tip. (c) Background subtracted CV of NB on ITO acquired concurrently with the EC-TER spectra in (a). $E^{0\prime}$ = −0.215 V. (d) Charge acquired by integrating the CV in (c). The charge is directly proportional to the number of molecules reduced during the CV. The reverse sweep is offset by 0.6 μC/cm^2 for clarity. (e) Potential dependence of the integrated TERS intensity of the 591 cm^{-1} band of NB_{OX}. The black lines are meant to highlight the dependence as a guide for the reader. The intensity−potential profiles strongly resemble the mirror image of the charge shown in (d). All TERS intensities were normalized to the initial value at 0.0 V vs Ag/AgCl. The reverse sweep is offset for clarity. TERS spectra in (a) and TERS voltammograms in (e) are the average of four experiments.

between the SER and TER spectra are listed in SI Table S1. We therefore have successfully demonstrated the first use of TERS to monitor structural changes of an electroactive species upon its reduction.

We then explored the use of TERS for studying the nanoscale voltammetric behavior of NB (Figure 3). Figure 3a and b show selected TER spectra acquired concurrently with the cyclic voltammogram (CV) in Figure 3c. As the potential is swept from 0.00 V to −0.60 V the overall intensities of the TERS spectra decrease, in agreement with the change in electronic resonance shown in Figure 1. As the potential is swept from −0.60 V back to 0.00 V, 75% of the initial TERS intensity returns, demonstrating that the nearly reversible redox chemistry of NB under the AFM tip monitored using TERS. The loss of ∼25% of the initial NB signal is consistent with the conventional CV and is likely due to reductive desorption of NB_{RED}, which is less strongly bound than NB_{OX}. Figure 3c shows the CV acquired during the TERS measurements in Figure 3a and b. The cathodic (E_{pc}) and anodic (E_{pa}) peaks are located at −0.24 V and −0.19 V vs Ag/AgCl, respectively, corresponding to a peak separation (ΔE_p) of 50 mV and $E^{0\prime}$ ∼ −0.215 V. By integrating the CV in Figure 3c, we obtain a charge vs potential curve, shown in Figure 3d. The amount of charge passed on the forward and backward sweeps is directly proportional to the number or molecules reduced and oxidized respectively (∼0.62 μC/cm^2 and 0.40 μC/cm^2 respectively, corresponding to 1.9 × 10^{12} molecules/cm^2, or ∼0.02 monolayer assuming NB lies flat on the surface with ∼1 molecule/nm^2). We therefore expect the disappearance of the NB_{OX} TERS signal to exhibit behavior opposite that of the charge, that is, the NB_{OX} TERS signal will decrease as the cathodic charge increases and increase as the anodic charge becomes more negative.

As the potential is scanned from 0 V vs Ag/AgCl to −0.6 V, the intensity of the 591 cm^{-1} band decreases beginning at ∼ −0.3 V (Figure 3e). It then decreases until ∼ −0.5 V, at which point the intensity levels off. Upon sweeping the potential back to 0 V vs Ag/AgCl, we observe that the intensity at 591 cm^{-1} begins to increase linearly at ∼ −0.4 V and levels off at ∼ −0.2 V. As expected, the TERS intensity−potential profile for the 591 cm^{-1} band strongly resembles the mirror image of the charge vs potential curve in Figure 3d. However, we observe a shift in the potentials at which reduction and oxidation occur as observed by TERS relative to the CV. Although the onset of the cathodic current in the CV occurs at ∼ −0.13 V, the TERS intensity does not begin to decrease until ∼ −0.3 V. Similarly, the onset of anodic current in the CV occurs at ∼ −0.3 V, whereas the TERS intensity begins to reappear at ∼ −0.4 V. Therefore, the TERS potential response is shifted more than 100 mV further negative than the conventional voltammetric response in Figure 3c. To verify that the shift of the optical response relative to the CV is specific to the near-field response, we have also monitored the fluorescence of NB on ITO and SERS of NB on Au. A full discussion of these results is provided in the Supporting Information (Figures S3 and S4).

Further, we observed that the TERS intensity−potential profiles from multiple experiments show nearly identical shifts relative to the conventional CV (vide infra). This consistency

DOI: 10.1021/acs.nanolett.5b04177
Nano Lett. 2015, 15, 7956−7962

suggests that the shift observed in the TERS voltammogram relative to the CV is likely the result of some perturbation by the tip rather than local variations in the formal potential ($E^{0\prime}$) across the electrode surface.[11,14] Specifically, reduction of NB in the tip−sample junction is energetically less favorable (oxidation is more favorable) than reduction (oxidation) across the bulk of the ITO surface. There are several possible explanations for the shift in the TERS response relative to the CV. A subensemble of NB molecules may be trapped between the AFM tip and the ITO surface, limiting the electrochemical accessibility of the NB molecules contributing to the TERS response. Alternatively, we hypothesize that the tip locally perturbs the structure of the compact layer in the electrical double-layer. Distortion of the double-layer structure locally alters the effective potential experienced by the NB molecules in the tip−sample junction such that a larger overpotential is required for reduction.

In light of the perturbation of the local interfacial structure by the tip discussed above, it is necessary to examine whether the tip impacts the heterogeneous electron transfer kinetics of the NB molecules directly beneath it. In Figure 3d, the potential by which half of the anodic charge has passed is −0.24 V vs Ag/AgCl (corresponding to E_{pc}), whereas the potential by which half of the catholic charge has passed is −0.19 V (corresponding to E_{pa}). Analogously, we define the cathodic TERS "peak potential" ($E_{pc,TERS}$) to be the potential by which half of the initial intensity at 591 cm^{-1} has been lost and the anodic TERS "peak potential" ($E_{pa,TERS}$) to be the potential by which half of the intensity has returned. Using these definitions, we find that $E_{pc,TERS}$ = −0.435 V vs Ag/AgCl and $E_{pa,TERS}$ = −0.290 V.

The voltammetric peak separation measured by TERS ($\Delta E_{p,TERS}$) is ∼145 mV, which is significantly larger than the 50 mV peak separation measured by conventional CV. This increase in peak separation suggests that the tip may also locally slow down the heterogeneous charge transfer kinetics in the junction or locally increase the uncompensated resistance.[32] To investigate whether the tip impacts the kinetics of NB reduction and oxidation in the tip−sample junction, we examined the dependence of the TERS intensity−potential profiles on scan rate.

TERS voltammograms were acquired using scan rates of 5, 10, 20, and 30 mV/s (Figure 4). For all four scan rates, the behavior of the intensity−potential profiles is nearly identical. If the tip did locally slow the charge transfer kinetics of NB, we would expect $\Delta E_{p,TERS}$ to increase as the scan rate increases.[32] However, no clear trend is observed in the behavior of $\Delta E_{p,TERS}$ as a function of scan rate. Therefore, we conclude that the kinetics of NB reduction and oxidation are not perturbed significantly enough to be detected in the TERS voltammogram within this range of scan rates. In conventional analysis of cyclic voltammetry, an increase in peak separation cannot be energetic in nature and must either correspond to slowed electron transfer kinetics or increased uncompensated resistance.[32] This contradiction between TERS voltammetry and conventional CV analysis suggests that the use of $E_{pc,TERS}$, $E_{pa,TERS}$, and $\Delta E_{p,TERS}$ as diagnostic parameters for nanoscale voltammetry requires more thorough consideration.

The major assumption in the definition of these three diagnostic parameters is that the TERS intensity is directly proportional to the number of molecules occupying the tip−sample junction. This is not necessarily the case. In order to understand the dependence of the TERS intensity on the number of molecules reduced or oxidized, one must consider the distribution of the enhanced electric field in the junction. Simulations of the field distribution in the hot spot beneath the tip have shown that the intensity of the electric field decays dramatically with increasing radial distance from the tip apex.[33] Although all molecules located in the tip−sample junction will contribute to the TERS intensity, those closest to the apex of the tip will experience the greatest enhancement, whereas those on the periphery will experience less. As such, not all molecules in the junction contribute equally to the TERS intensity. Thus, it is reasonable to expect that although the TERS intensity−potential profile in Figure 3e strongly resembles the mirror image of the charge vs potential curve in Figure 3d, the quantitative relationship between the two curves is not straightforward without precise knowledge of the distribution of molecules within the hot spot.

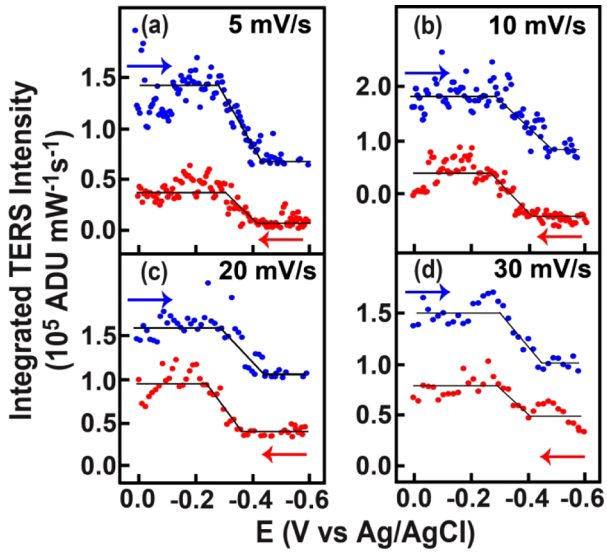

Figure 4. TERS voltammograms acquired as a function of scan rate (5 mV/s, 10 mV/s, 20 mV/s, and 30 mV/s in (a)−(d), respectively). The black lines drawn through the data points are meant as a guide for the reader. The arrows in the upper left and lower right of each panel mark the initial potential and scan direction of the forward and backward sweeps, respectively. The backward sweeps for all scan rates are offset for clarity.

Further, because TERS is a nanoscale measurement, very few molecules are being probed in our EC-TERS experiments. The surface excess of NB on the ITO surface determined from integration of the CV (vide supra) is 1.9×10^{12} molecules/cm^2 (∼0.02 monolayer). To estimate an upper limit for the number of molecules probed in our EC-TERS experiments, we assume that TERS probes a circular area with radius (R_{TERS}) equal to half of the tip radius of curvature (R_{Tip} = 20 nm).[34] Using these criteria, we estimate that fewer than 10 molecules are probed in our EC-TERS experiments. It is reasonable to expect that the subensemble of NB molecules contributing to the TERS voltammogram will not have directly analogous behavior to the thermodynamic distribution probed by conventional CV. Therefore, although $E_{pc,TERS}$, $E_{pa,TERS}$, and $\Delta E_{p,TERS}$ are seemingly reasonable diagnostic parameters analogous to those typically used in conventional voltammetry, theoretical relationships between TERS intensity and charge must be developed in order to properly analyze nanoscale TERS voltammetric data. A thorough investigation of the behavior

DOI: 10.1021/acs.nanolett.5b04177
Nano Lett. 2015, 15, 7956−7962

of TERS voltammetry compared to conventional voltammetry is currently underway in our laboratory.

We have directly observed the electrochemical behavior of few NB molecules consistent with our coverage estimate (vide supra). TERS voltammograms were acquired at four different locations on the ITO surface as a proof of concept for spectroelectrochemical TER mapping (Figure 5). In some of the TERS voltammograms (most prominently in Figure 5b), there are clearly step-like features corresponding to the reduction and oxidation of single or few molecules. In contrast, the TERS voltammogram in Figure 5d shows a continuous linear response. We hypothesize that the coverage of NB on the ITO surface is nonuniform. In areas of lower coverage (perhaps where isolated molecules are adsorbed), step-like behavior is observed as individual or few molecules are reduced and oxidized. In areas with higher coverage, the behavior of the individual molecules cannot be resolved, and the linear potential response resembles that of the ensemble fluorescence and SERS measurements in SI Figures S3 and S4. Differentiating between regions of different coverage across the ITO surface can only be achieved by controlling the location of the TERS hot spot. Such information is inaccessible by traditional electrochemical methods (e.g., cyclic voltammetry) and spectroscopic techniques (e.g., gap-mode SERS).

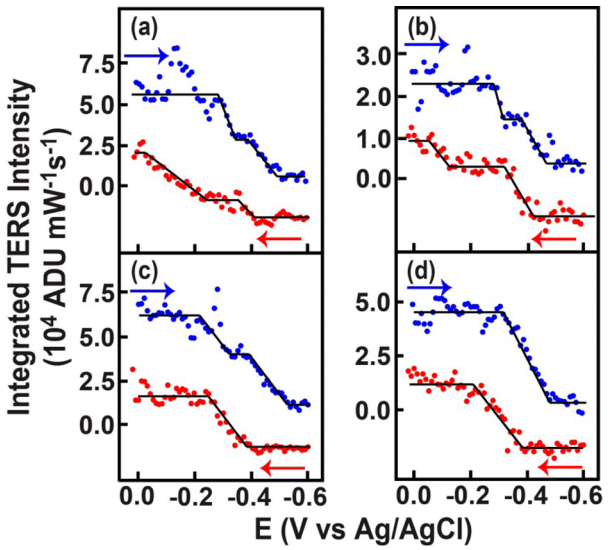

Figure 5. TERS voltammograms acquired at four different locations (panels a–d) on the ITO surface. Three of the voltammograms (particularly panel b) show step-like behavior indicative of single or few molecule electrochemistry. In contrast, panel d shows a linear response corresponding to a higher local coverage of NB.

We have successfully demonstrated the first use of EC-TERS to study the 2 e^-, 1 H^+ reaction of NB. We used EC-TERS to monitor the structural changes of NB upon its reduction and at a particular point of interest in the electrode surface. Further, we have examined the influence of the tip on the electrochemistry occurring directly beneath it and have concluded that although the tip locally perturbs the structure of the electrical double-layer, it has no detectable impact on the electron transfer kinetics. Additionally, we observed step-like features in some of the TERS voltammograms that correspond to the reduction and oxidation of single or few NB molecules on the ITO surface. The step-like behavior is observed at some locations on the ITO surface, but not all, indicating that the coverage of NB across the ITO surface is not uniform. Extension of EC-TERS to tapping mode AFM and shear force AFM platforms is currently underway in our lab in order to more deeply understand the effects of the TERS tip on the electrochemical processes occurring in the tip–sample junction. Overcoming the current challenges to EC-TERS will allow for chemically specific mapping of electrochemical interfaces at the nanoscale, a problem of particular interest for the development of novel electrocatalysts and devices for renewable energy production and storage.

■ ASSOCIATED CONTENT

Supporting Information

The Supporting Information is available free of charge on the ACS Publications website at DOI: 10.1021/acs.nanolett.5b04177.

Figures S1–S10 and Table S1: A schematic of the EC-TERS instrument, discussion of tip contamination, table of Nile blue Raman modes with mode assignments, raw cyclic voltammograms corresponding to Figures 3C and 4, a comparison of NB voltammograms on ITO and Au, an AFM image of the ITO electrode, a discussion of background subtraction of the CVs, SERS and fluorescence far-field control experiments, TERS voltammograms using the 1193 and 1376 cm^{-1} modes of NB, and the calculation of the TERS enhancement factor. (PDF)

■ AUTHOR INFORMATION

Corresponding Author

*E-mail: vanduyne@northwestern.edu.

Author Contributions

Dmitry Kurouski and Michael Mattei contributed equally to this work.

Notes

The authors declare no competing financial interest.

■ ACKNOWLEDGMENTS

This work was supported by the Air Force Office of Scientific Research MURI (FA9550-14-1-0003). The authors thank Dr. Guillaume Goubert, Stephanie Zaleski, and Naihao Chiang for helpful discussions.

■ REFERENCES

(1) Bard, A. J. *J. Am. Chem. Soc.* **2010**, *132*, 7559–7567.
(2) Huang, X.; Zhao, Z.; Cao, L.; Chen, Y.; Zhu, E.; Lin, Z.; Li, M.; Yan, A.; Zettl, A.; Wang, Y. M.; Duan, X.; Mueller, T.; Huang, Y. *Science* **2015**, *348*, 1230–1234.
(3) Neurock, M.; Janik, M.; Wieckowski, A. *Faraday Discuss.* **2009**, *140*, 363–378.
(4) Spendelow, J. S.; Wieckowski, A. *Phys. Chem. Chem. Phys.* **2007**, *9*, 2654–2675.
(5) Spendelow, J. S.; Xu, Q.; Goodpaster, J. D.; Kenis, P. J. A.; Wieckowski, A. *J. Electrochem. Soc.* **2007**, *154*, F238–F242.
(6) Johnson, R. P.; Fleming, A. M.; Jin, Q.; Burrows, C. J.; White, H. W. *Biophys. J.* **2014**, *107*, 924–931.
(7) Bard, A. J.; Fan, F. F.; Kwak, J.; Lev, O. *Anal. Chem.* **1989**, *61*, 132–138.
(8) Sun, T.; Yu, Y.; Zacher, B. J.; Mirkin, M. V. *Angew. Chem., Int. Ed.* **2014**, *53*, 14120–14123.
(9) Wilms, M.; Kruft, M.; Bermes, G.; Wandelt, K. *Rev. Sci. Instrum.* **1999**, *70*, 3641–3650.

DOI: 10.1021/acs.nanolett.5b04177
Nano Lett. 2015, 15, 7956–7962

(10) Yoshimoto, S.; Itaya, K. *Annu. Rev. Anal. Chem.* **2013**, *6*, 213−235.
(11) Cortés, E.; Etchegoin, P. G.; Le Ru, E. C.; Fainstein, A.; Vela, M. E.; Salvarezza, R. C. *J. Am. Chem. Soc.* **2010**, *132*, 18034−18037.
(12) Cortés, E.; Etchegoin, P. G.; Le Ru, E. C.; Fainstein, A.; Vela, M. E.; Salvarezza, R. C. *J. Am. Chem. Soc.* **2013**, *135*, 2809−2815.
(13) Renault, C.; Marchuk, K.; Ahn, H. S.; Titus, E. J.; Kim, J.; Willets, K. A.; Bard, A. J. *Anal. Chem.* **2015**, *87*, 5730−5737.
(14) Wilson, A. J.; Willets, K. A. *Nano Lett.* **2014**, *14*, 939−945.
(15) Chen, C.; Hayazawa, N.; Kawata, S. *Nat. Commun.* **2014**, *5*, 3312−3316.
(16) Klingsporn, J. M.; Jiang, N.; Pozzi, E. A.; Sonntag, M. D.; Chulhai, D.; Seideman, T.; Jensen, L.; Hersam, M. C.; Van Duyne, R. P. *J. Am. Chem. Soc.* **2014**, *136*, 3881−3887.
(17) Kurouski, D.; Deckert-Gaudig, T.; Deckert, V.; Lednev, I. K. *J. Am. Chem. Soc.* **2012**, *134*, 13323−13329.
(18) Kurouski, D.; Zaleski, S.; Casadio, F.; Van Duyne, R. P.; Shah, N. C. *J. Am. Chem. Soc.* **2014**, *136*, 8677−8684.
(19) Schmid, T.; Opilik, L.; Blum, C.; Zenobi, R. *Angew. Chem., Int. Ed.* **2013**, *52*, 5940−5954.
(20) Jiang, S.; Zhang, Y.; Zhang, R.; Hu, C.; Liao, M.; Luo, Y.; Yang, J. L.; Dong, Z. C.; Hou, J. G. *Nat. Nanotechnol.* **2015**, *10*, 865−869.
(21) Sonntag, M. D.; Chulhai, D.; Seideman, T.; Jensen, L.; Van Duyne, R. P. *J. Am. Chem. Soc.* **2013**, *135*, 17187−17192.
(22) Sonntag, M. D.; Klingsporn, J. M.; Garibay, L. K.; Roberts, J. M.; Dieringer, J. A.; Seideman, T.; Scheidt, K. A.; Jensen, L.; Schatz, G. C.; Van Duyne, R. P. *J. Phys. Chem. C* **2012**, *116*, 478−483.
(23) Zhang, R.; Zhang, Y.; Dong, Z. C.; Jiang, S.; Zhang, C.; Chen, L. G.; Zhang, L.; Liao, Y.; Aizpurua, J.; Luo, Y.; Yang, J. L.; Hou, J. G. *Nature* **2013**, *498*, 82−86.
(24) Kumar, N.; Stephanidis, B.; Zenobi, R.; Wain, A. J.; Roy, D. *Nanoscale* **2015**, *7*, 7133−7137.
(25) van Schrojenstein Lantman, E. M.; Deckert-Gaudig, T.; Mank, A. J. G.; Deckert, V.; Weckhuysen, B. M. *Nat. Nanotechnol.* **2012**, *7*, 583−586.
(26) Zhang, Z. L.; Chen, L.; Sun, M. T.; Ruan, P. P.; Zheng, H. R.; Xu, H. X. *Nanoscale* **2013**, *5*, 3249−3252.
(27) Schmid, T.; Yeo, B.; Leong, G.; Stadler, J.; Zenobi, R. *J. Raman Spectrosc.* **2009**, *40*, 1392−1399.
(28) Zeng, Z.; Huang, S.; Wu, D.; Meng, L.; Li, M.; Huang, T.; Zhong, J.; Wang, X.; Yang, Z.; Ren, B. *J. Am. Chem. Soc.* **2015**, *137*, 11928−11931.
(29) Greeneltch, N. G.; Blaber, M. G.; Henry, A. I.; Schatz, G. C.; Van Duyne, R. P. *Anal. Chem.* **2013**, *85*, 2297−2303.
(30) Ni, F.; Feng, H.; Gorton, L.; Cotton, T. M. *Langmuir* **1990**, *6*, 66−73.
(31) Cortés, E.; Etchegoin, P. G.; Le Ru, E. C.; Fainstein, A.; Vela, M. E.; Salvarezza, R. C. *Anal. Chem.* **2010**, *82*, 6919−6925.
(32) Bard, A. J.; Faulkner, L. R. *Electrochemical Methods: Fundamentals and Applications*; Wiley: New York, 2000.
(33) Downes, A.; Salter, D.; Elfick, A. *J. Phys. Chem. B* **2006**, *110*, 6692−6698.
(34) Pettinger, B.; Ren, B.; Picardi, G.; Schuster, R.; Ertl, G. *J. Raman Spectrosc.* **2005**, *36*, 541−550.

DOI: 10.1021/acs.nanolett.5b04177
Nano Lett. 2015, 15, 7956−7962